HOT MWIR InAs/InAsSb T2SL Discrete Photodetector Development

Jongwoo Kim,[1] Henry Yuan,[1] Joe Kimchi,[1] JihFen Lei,[1] Elizabeth Rangel,[2] Peter Dreiske,[2] and Amal Ikhlassi [3]

1. Teledyne Judson Technologies, 221 Commerce Drive, Montgomeryville, PA 18936
2. Teledyne Imaging Sensors, 5212 Verdugo Way, Camarillo, CA 93012
3. Teledyne Scientific Company, 1049 Camino Dos Rios, Thousand Oaks, CA 91360

ABSTRACT

Teledyne Judson Technologies (TJT) has developed high operating temperature (HOT) mid-wavelength infrared (MWIR) photodetectors based on InAs/InAsSb type-II superlattice (T2SL) with an electron barrier. Large area discrete detectors of 0.25mm and 1mm diameters were designed and fabricated for front-side illumination. Comprehensive E-O characterization was performed at room temperature and thermo-electric cooled (TEC) temperatures. The unique fabrication process was developed for a quasi-planar structure, enabling simplified fabrication for low-cost large volume production. The detector shows a 50% cut-off wavelength of ~5.5μm at room temperature. Peak responsivity of 2.47 A/W was achieved on 1mm detectors at peak wavelength ~4.24μm, -0.3V bias and 295K. Peak quantum efficiency (QE) was 72% with an antireflection coating. The 1mm detectors showed peak detectivity (D*) of 1.9×10^9 cm-√Hz/W at -0.3V bias, 295K and 10 kHz. Dark current density as low as 1.17 A/cm^2 was achieved at -0.3V bias and 295K on 1mm detectors. The dark current was diffusion-limited at higher temperatures above ~120K while it was dominated by either tunneling or surface leakage currents at lower temperatures. Similar results were obtained on 0.25mm detectors.

Keywords: HOT, MWIR, InAs/InAsSb, T2SL, Discrete Photodetector

1. INTRODUCTION

InAs/InGaSb T2SLs have been extensively studied as an alternative material system to HgCdTe for MWIR detection for use in a variety of military, industrial, and medical applications [1,2,3]. These include thermal imaging, chemical sensing, and medical diagnostics. The band structure of T2SLs can be tailored to create desired bandgap by varying the constituent layer thickness and composition and thus providing wide design flexibility. Several different types of the device hetero-structures have been proposed to reduce dark current such as nBn [4], complimentary-barrier infrared detector (CBIRD) [5], M-structure [6], W-structure [7], N-structure [8], and pBiBn [9]. It has been predicted that InAs/InGaSb T2SLs can offer potentially detector performance comparable or similar to HgCdTe [10]. They have smaller tunneling currents due to higher effective mass of electrons and holes. Auger recombination is suppressed by spatially indirect electron and hole wave functions and large strain-induced splitting between heavy-hole and light-hole subbands. The suppression of Auger recombination increases carrier lifetime and leads to low dark currents and high operating temperatures. However, the InAs/InGaSb T2SL detectors have not shown the predicted performance because of difficulty in material growth, device fabrication process, and device passivation. The carrier lifetime of InAs/InGaSb T2SLs is limited by the Shockley-Read-Hall (SRH) recombination mechanism. To overcome this, much attention has been recently given to Ga-free InAs/InAsSb T2SL system as a candidate material for infrared detectors because InAs/InAsSb T2SLs has a longer carrier lifetime compared to InAs/InGaSb T2SLs [11, 12]. Carrier lifetime of 500ns at 77K was reported in longwave infrared InAs/InAsSb T2SLs detectors [13, 14].

In this paper, we report the device design and fabrication process of InAs/InAsSb T2SL discrete detectors and discuss their potential for high operating temperature MWIR photodetector applications. Comprehensive E-O characterization was performed at room temperature and TEC temperatures. Different device structures were investigated to study the dark current and optical performance of the detectors. The unique fabrication process was developed for a quasi-planar structure, enabling simplified fabrication for low-cost large volume production. Relatively high detector performance was achieved at room temperature and TEC temperatures, close to that of conventional MWIR HgCdTe discrete photodiodes.

2. DETECTOR FABRICATION

2.1 STRAINED LAYER SUPERLATTICE (SLS) STRUCTURE AND GROWTH

InAs/$InAs_{0.6}Sb_{0.4}$ T2SL MWIR detectors were designed using an electron barrier to give ~5.5μm cutoff wavelength at room temperature. Figure 1 shows a schematic of the device structure. The device consists of an n-type doped top T2SL contact layer, a barrier layer, an undoped InAs/InAsSb T2SL absorber, and an n-type doped bottom contact layer on n-type GaSb substrate. All the T2SL layers consist of the same number of monolayers (MLs) of InAs and InAsSb.

The wafer was grown at Teledyne Scientific Company (TSC) by molecular beam epitaxy (MBE) on 3" n-type Te-doped (100) GaSb substrates. High-resolution X-ray diffraction was used to study the structural quality and strain properties of InAs/InAsSb SLS structure. Figure 2(a) shows X-ray rocking curve of a properly designed MLs of InAs/$InAs_{0.6}Sb_{0.4}$ SLS structure. Well-resolved satellite peaks are observed. The full width at half maximum (FWHM) of GaSb buffer and the zeroth order superlattice peak are 18 and 20.16 arcseconds. The measured lattice mismatch between the SLS and GaSb substrate is $\Delta a/a = -9.22 \times 10^{-4}$ indicating that the SLS structure is under compressive strain. Figure 2(b) shows photoluminescence (PL) data of the SLS structure. PL measurement was performed at 78K with a 1550nm laser modulated at 25 kHz and cooled InSb photodetector. The peak PL wavelength was 4.67μm with FWHM of 26.3meV.

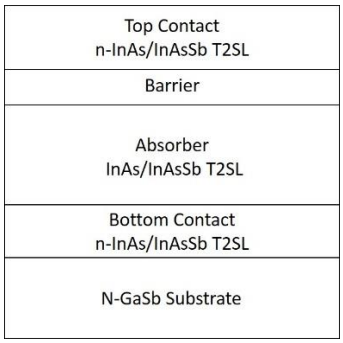

Fig. 1. Device structure of MWIR InAs/InAsSb T2SL detectors.

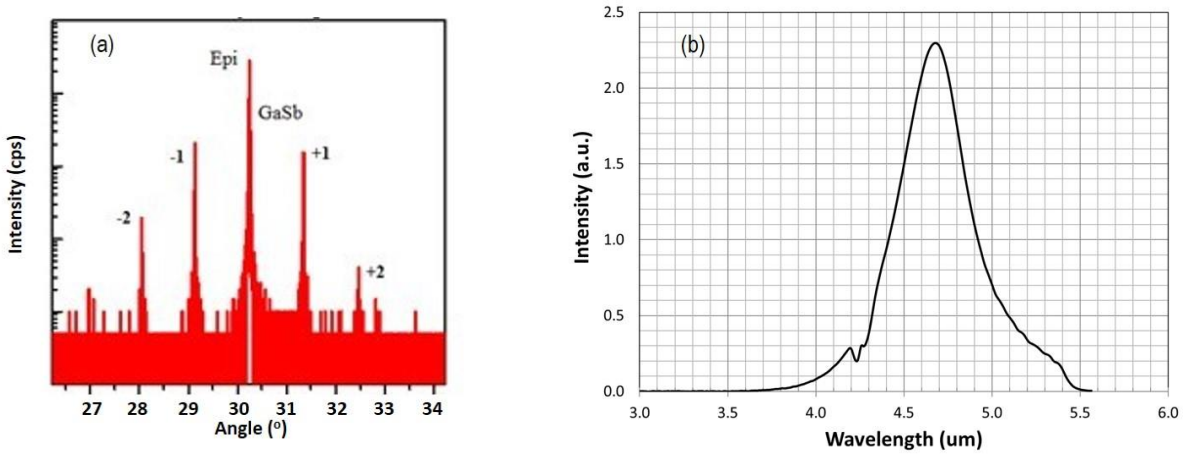

Fig. 2. X-ray rocking curve (a) and PL spectrum (b) of MWIR InAs/InAsSb T2SL structure. PL measurement was performed at 78K using 1550nm laser modulated at 25 kHz with cooled InSb detector.

2.2 DEVICE STRUCTURE AND PROCESSING

Large size discrete detectors of 0.25mm and 1mm diameters were fabricated for front-side illumination using standard photolithography technique. Performance evaluation chips (PECs) were included to investigate different device structures and various test devices with different sizes and geometry. The mesas were first wet etched. The etching was stopped at the top of the barrier layer. The sidewall of mesas was passivated by a SiO_2 layer deposited at low temperature using plasma enhanced chemical vapor deposition (PECVD) system. Contact windows were opened using wet etching. An antireflection coating layer and the metal contacts were then deposited using an e-beam evaporator. Figure 3 shows a photo of a completed photodetector.

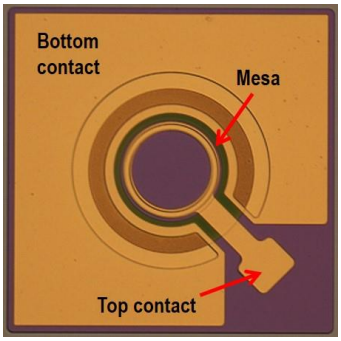

Fig. 3. Photo of a completed front-illuminated InAs/InAsSb T2SL detectors.

2.3 DEVICE CHARACTERIZATION

The electrical and optical properties of InAs/InAsSb T2SL detectors were characterized using current-voltage (I-V) and spectral response measurements. The detector chips were mounted on ceramic carriers and then packaged in the flat pack and wire bonded. The flat pack was loaded into a variable temperature dewar for low temperature measurements. For the dark current measurements, a thermal shield was used to cover the detector in order to block the background infrared radiation. The spectral response of the detectors was measured using Nexus 6700 Fourier transform infrared (FTIR) spectrometer with TJT's PA-6 preamplifier at various biases and temperatures. To calculate absolute responsivity and QE of the T2SL detectors, a focused spot scan measurement was performed with a 1000K blackbody source with chopper and aperture, a narrow band pass filter, a calibrated reference standard InSb detector, and HP dynamic signal analyzer (DSA) in an optical test bench. Similarly PA-6 preamplifier and DSA were used to measure the noise spectral density of the detectors.

3. RESULTS AND DISCUSSION

The dark current was measured as a function of bias and temperature. Figure 4 (a) and (b) show the dark current density of 0.25mm and 1mm MWIR InAs/InAsSb T2SL detectors, respectively. The dark current densities of 0.25mm detector at 208K and 295K under -0.1V bias voltage were measured as 4.17×10^{-3} A/cm^2 and 1.48 A/cm^2, respectively. The lowest dark current density achieved from 0.25mm detectors was 1.34 A/cm^2 at 295K. Similarly, 1mm detectors showed the dark current density as low as 1.17 A/cm^2 at -0.3V at the temperature of 295K.

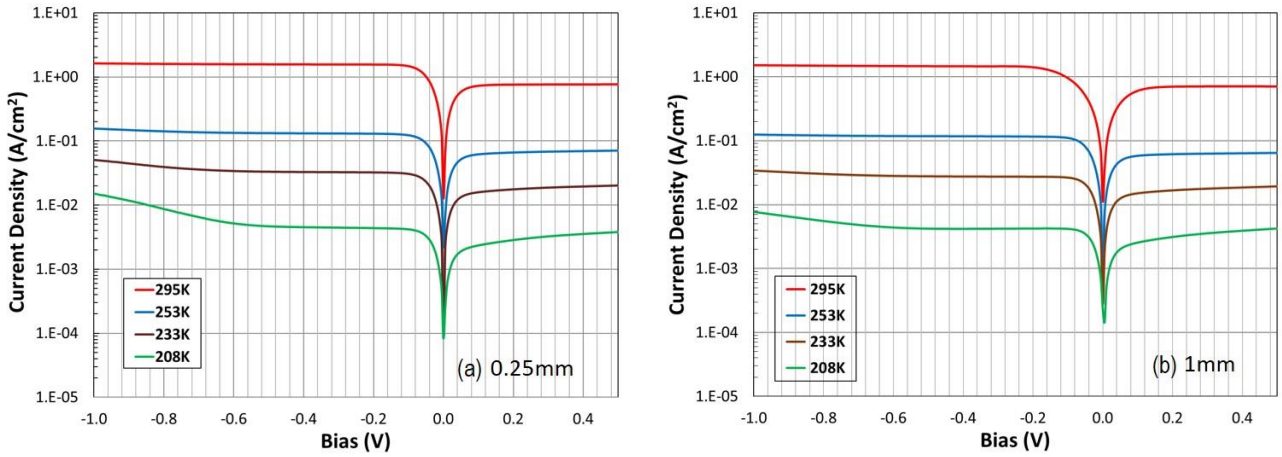

Fig. 4. Temperature dependent dark current density of 0.25mm and 1mm InAs/InAsSb T2SL detectors.

The activation energy was calculated from the temperature dependent dark current. Figure 5 (a) shows the Arrhenius plot of 0.25mm detector. At high temperatures above ~120K, the activation energy E_a is 279 meV which is close to the energy gap of InAs/InAsSb T2SL structure. This indicates that the dark current is dominated by diffusion current at high temperatures. At low temperatures below ~120K, the activation energy is 19 meV, much less than the bandgap energy indicating the dark current is dominated by either tunneling or surface leakage currents. The differential resistance-area product of the 0.25mm detector measured at -0.2V was 175 Ωcm^2 at 208K and 0.27 Ωcm^2 at 295K. Surface resistivity was also calculated from the slope of the inverse dynamic resistance-area product as a function of perimeter to area ratio at 295K and -0.3V, as shown in Figure 5 (b). The surface resistivity was 1.4 x10^3 Ωcm. This low surface resistivity may be attributed to either the surface leakage current from poor surface passivation or lateral collection of carriers due to shallow etched device structure. In the current shallow etched devices, carriers can be collected laterally from the surrounding areas because there is no physical definition of the device. We are currently investigating ways to improve the surface passivation and reduce lateral collection of carriers.

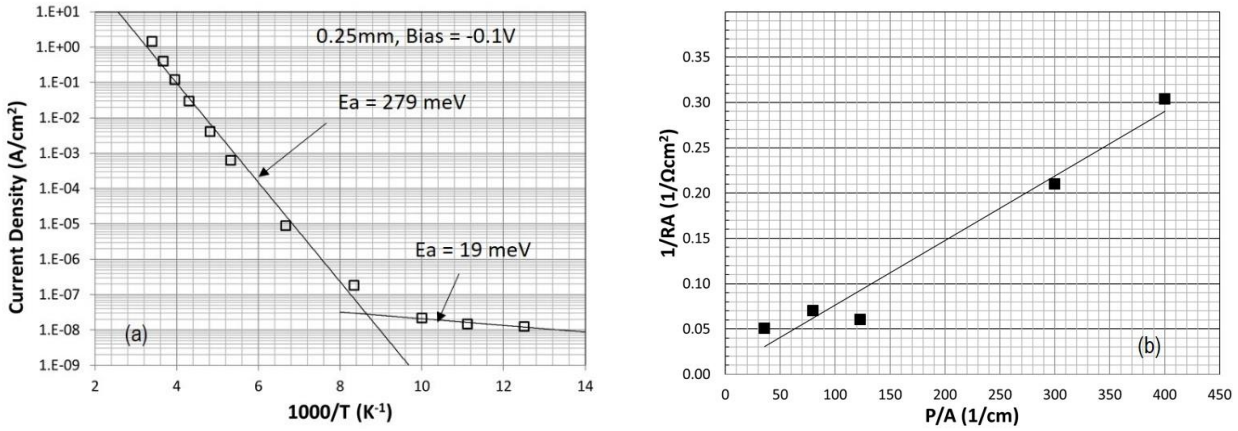

Fig. 5. Arrhenius plot (a) of 0.25mm MWIR InAs/InAsSb T2SL detector. For temperature above ~120K, Ea is 279 meV, indicating diffusion current is dominant. (b) Dynamic resistance-area product at -0.3V vs perimeter to area ratio at 295K.

The spectral response characteristics of 0.25mm and 1mm detectors were measured as a function of temperature from 208K to 295K. Figure 6 (a) and (b) show the responsivity and QE of the 1mm detector measured at -0.3V. The 50% cutoff wavelength of the detector was 4.93μm at 208K, which increased to 5.36μm at 295K. The peak responsivity was measured as 2.23 A/cm^2 at 4.01μm and 208K. At 295K, the peak responsivity slightly increased to 2.34 A/cm^2. The corresponding values of QE at the peak responsivity were 68.9% at 208K and 70% at 295K. The maximum peak responsivity and QE of 1mm detectors at 295K were 2.47 A/cm^2 and 72% at 4.24μm, respectively. It can be seen in Figure 7 that the peak responsivity and QE are relatively insensitive to the temperature in the range of 208K to 295K. 0.25mm detectors showed comparable performance to 1mm detectors (not shown). The peak responsivity was 2.05 A/cm^2 at -0.2V bias and 295K, corresponding to the QE of 60% at 4.24μm.

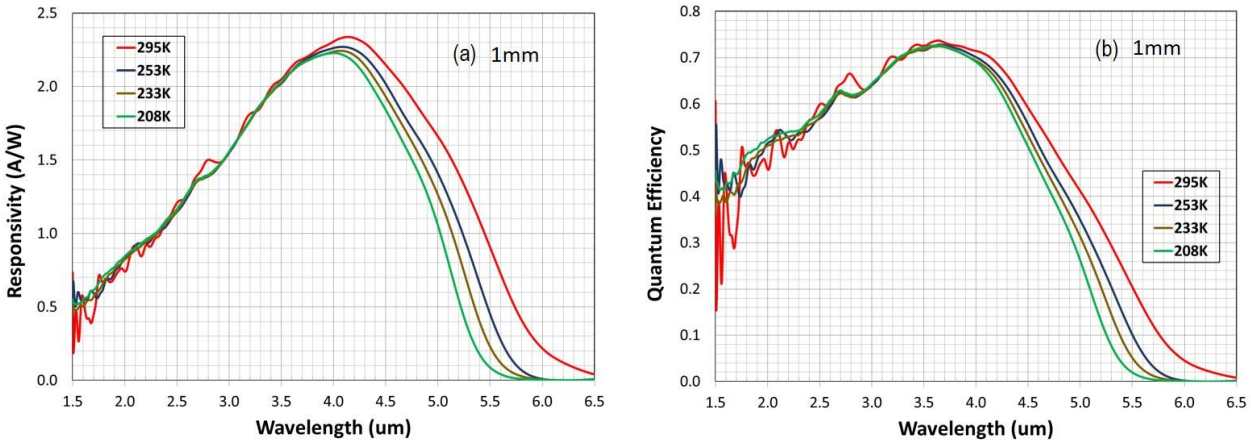

Fig. 6. Temperature dependent responsivity (a) and quantum efficiency (b) of large size 1mm InAs/InAsSb T2SL detector. A peak responsivity (a) and corresponding QE (b) as a function of temperature.

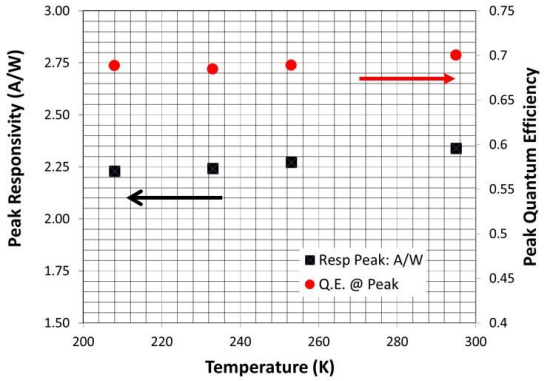

Fig. 7. Temperature dependence of the peak responsivity and corresponding QE of 1mm detector. The detector was biased at -0.3V. The optical performance exhibited little change with temperature.

Figure 8 shows the noise spectra for 0.25mm (a) and 1mm (b) detectors. The noise was measured at 295K. A 0.25mm detector was biased at -0.2V and the noise was measured as 28.84nV/Hz$^{1/2}$ at 10 kHz. The value of Johnson noise of the detector was 0.09nV/Hz$^{1/2}$. The noise was dominated by shot noise of the detectors. The noise output for a 1mm detector,

measured at -0.3V bias, was 18.24nV/Hz$^{1/2}$. It is clearly seen in Figure 8 that the InAs/InAsSb type II detectors have low 1/f noise.

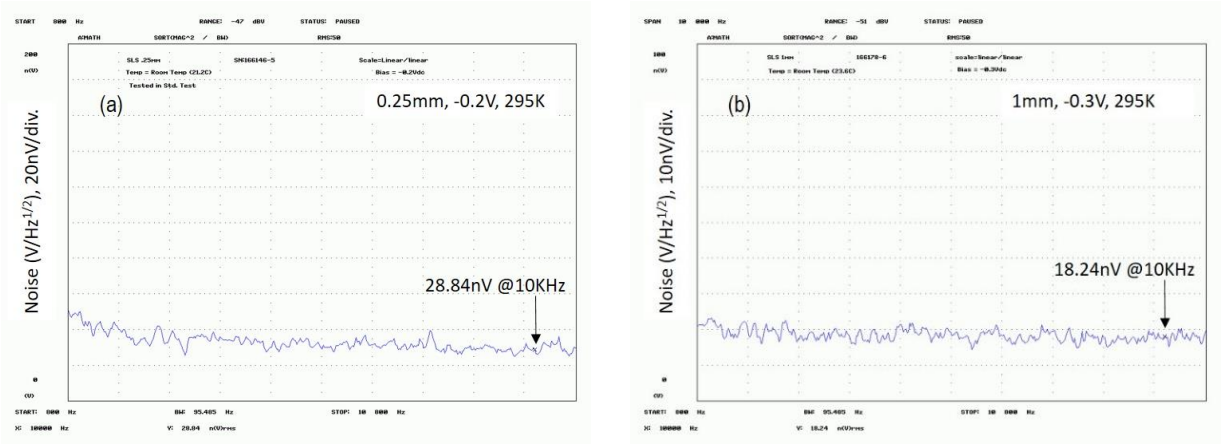

Figure 8. The measured output noise spectra for 0.25mm (a) and 1mm (b) detectors. The measured noise voltage was 28.84nV/Hz$^{1/2}$ at -0.2V for 0.25mm detector and 18.24nV/Hz$^{1/2}$ at -0.3V for 1mm detector at the temperature of 295K.

Figure 9 shows the temperature dependent specific detectivity (D*) spectrum of 0.25mm and 1mm detectors. Detectivity was calculated using the noise spectral density measured at 10 kHz and -0.2V bias for 0.25mm detector (Fig. 9 (a)) and -0.3V bias for 1mm detector (Fig. 9 (b)). When the temperature decreases, the detectivity improved steadily due to lower dark currents and thus less noise while the responsivity and QE showed little changes with temperature. Both detectors exhibited a similar D* behavior. At 208K, the 0.25mm device showed a peak D* of 2.81x10^{10} cm-√Hz/W (Jones) at -0.2V and 4.08μm. At 295K, D* was reduced to 1.44x10^{9} cm-√Hz/W at -0.2V and 4.24μm. Similarly, the 1mm device exhibited a peak D* of 4.89x10^{10} cm-√Hz/W at -0.3V, 4.01μm, and 208K while at 295K, detectivity was 1.93x10^{9} cm-√Hz/W at -0.3V and 4.14μm. The measured D* values are compared with the D* values calculated theoretically by assuming that Johnson noise and shot noise are dominant. A theoretical D* for 1mm detector at 295K is expected to be 3.04x10^{9} cm-√Hz/W which is larger than the measured D*. This can be attributed to the noise due to other dark current mechanisms as well as the test system noise.

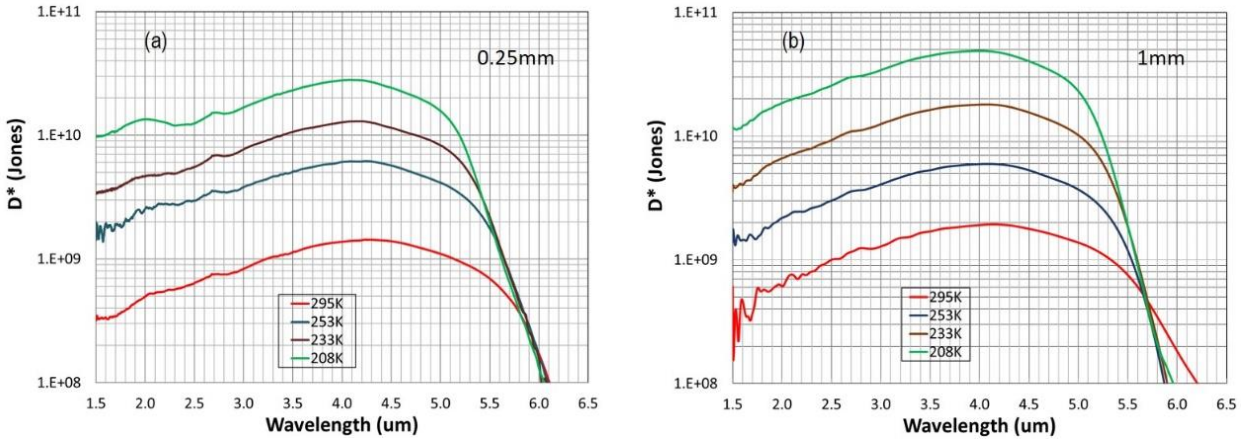

Fig. 9. Specific detectivity spectrum (D*) of the 0.25mm (a) and 1mm (b) detectors as a function of temperature ranging from 208K to 295K. D* was calculated based on the noise measured at -0.2V for 0.25mm and -0.3V for 1mm detector.

The detector showed good spatial uniformity of response as shown by the focused spot scan 3D plots (not shown). In this test, the detectors were operated at -0.3V bias at room temperature, with a 1.55μm laser diode modulated at 1kHz and a spot size of about 20μm. The 0.25mm detector exhibited the non-uniformity of photo-response over the entire active area less than 5% while the 1mm detector showed the response non-uniformity less than 8%. This spatial response non-uniformity can be attributed to the high sheet resistance of the top contact SLS layer.

4. CONCLUSION

In summary, we have reported the device design, fabrication process, and characterization of high performance large discrete MWIR photodetectors based on InAs/InAsSb T2SL structure on GaSb substrates. The front-side illuminated 1mm detector showed a 50% cutoff wavelength of ~5.5μm at 295K, a peak responsivity of 2.47 A/W at 4.24μm and -0.3V bias, corresponding QE of 72% with an antireflection coating. The dark current density of 1mm detectors was as low as 1.17 A/cm^2 at -0.3V bias voltage and 295K. A detectivity of 1.93×10^9 cm-√Hz/W was achieved on 1mm detector at -0.3V and 295K. The diffusion-limited dark current was achieved at higher temperatures above ~120K while the dark current was dominated by either tunneling or surface leakage at lower temperatures. Similar results were obtained on 0.25mm detectors. Although the detectors exhibited good optical performance, the dark current was still large. Further dark current reduction can be achieved with optimization of the device structure and fabrication processes. The relatively low cost and high performance make TJT's MWIR T2SL detectors a potentially good candidate for many applications that require room temperature or near room temperature operation.

ACKNOWLEDGEMENT

Authors would like to acknowledge internal research and development funding by Teledyne Imaging & Scientific and also thank Philip Bey, Indulis Graufelds, Dave Bond, Andrey Rumyantsev, James Edelman, and Kai Song for their support and testing T2SL detectors.

REFERENCES

[1] D.L. Smith, C. Mailhiot, "Proposal for strained type II infrared detectors," J. Appl. Phys. **62**, 2545 (1987)

[2] Y. Wei, A. Hood, H. Yau, Aaron Gin, M. Razeghi, "Unclooed operation of type-II InAs/GaSb superlattice photodiodes in the wavelength infrared range," Appl. Phys. Lett. **86**, 1 (2005)

[3] H.S.Kim, E. Plis, J. B. Rodriguez, G. D. Bishop, Y. D. Sharma, L. R. Dawson, S. Krishna, J. Bundas, R. Cook, D. Burrows, R. Dennis, K. Patnaude, A. Reisinger, M. Sundaram, "Mid-IR focal plane array based on type-II InAs/GaSb strain layer superlattice detector with nBn design," Appl. Phys. Lett. **92**, 1 (2008)

[4] J. B. Rodriguez, E. Plis, G. Bishop, Y. D. Sharma, H. Kim, L. R.. Dawson, S. Krishna, "NBn structure based on InAs/GaSb type-II strained layer superlattices," Appl. Phys. Lett. **91**, Article ID 043514 (2008)

[5] D.Z. Y. Ting, C. J. Hill, A. Soibel, S. A. Keo, J. M. Mumolo, J. Nguyen, S. D. Gunapala, "A high-performance long wavelength superlattice complementary barrier infrared detector," Appl. Phys. Lett. **95**, Article ID 023508 (2009)

[6] B. M. Nguyen, D. Hoffman, P. Y. Delaunay, M. Razeghi, "Dark current suppression in type-II InAs/GaSb superlattice long wavelength infrared photodiodes with M-structure barrier," Appl. Phys. Lett. **91**, Article ID 163511 (2007)

[7] E. H. Aifer, J. H. Warner, C. L. Canedy, I. Vurgaftman, E. M. Jackson, J. G. Tischler, J. R. Meyer, S. P. Powell, K. Olver, W. E. Tennant, "Shallow-etch mesa isolation of graded-bandgap W-structured type II superlattice photodiodes," J. Electron. Mater. **39**, 1070 (2010)

[8] O. Salihoglu, A. Muti, K. Kutluer, T. Tansel, R. Turan, Y. Ergun, A. Aydinli, "N-structure for type-II superlattice photodetectors," Appl. Phys. Lett. **101**, Article ID 073505 (2012)

[9] N. Gautam, H. S. Kim, M. N. Kutty, E. Plis, L. R. Dawson, S. Krishna, "Performance improvement of longwave infrared photodector based on type-II InAs/GaSb superlattices using unipolar current blocking layers," Appl. Phys. Lett. **96**, Article ID 231107 (2010)

[10] A. Rogalski, P. Martyniuk, M. Kopytko, "InAs/GaSb type-II superlattice infrared detectors: Future prospect," Appl. Phys. Rev. **4**, Article ID 031304 (2017)

[11] A. Haddadi, G. Chen, R. Chevallier, A. M. Hoang, M. Razeghi, "InAs/InAs1-xSbx type-II superalattices for high performance long wavelength infrared detection," Appl. Phys. Lett. **105**, Article ID 121104 (2014)

[12] A. Haddadi, R. Chevallier, G. Chen, A. M. Hoang, M. Razeghi, "Bias-selectable dual-band mid-/long-wavelength infrared photodetectors based on InAs/InAs1-xSbx type-II superlattices," Appl. Phys. Lett. **106**, Article ID 011104 (2015)

[13] Steenbergen, E.H., Connelly , B. C., Mtcalfe, G. D., Shen, H., Wraback, D. Lubyshev, Y. Qui, J. M. Fastenau, Liu, A. W. K., Elhamri, S., Cellek, O. O., Zhang, Y. H., "Significantly improved minority carrier lifetime observed in a long-wavelength infrared III-V type-II superlattice comprised of InAs/InAsSb," Appl. Phys. Lett. **99**, 251110 (2011)

[14] E.H. Steenbergen., B. C. Connelly, G. D. Mtcalfe, H. Shen, Wraback, M., Lubyshev, D., Qui, Y., Fastenau, J. M., A. W. K., Liu, S. Elhamri, O.O. Cellek, Y. H. Zhang, "Temperature-dependent minority carrier lifetimes of $InAs/InAs_{1-x}Sb_x$ type-II superlattices," Appl. Phys. Lett. **99**, 251110 (2011)